*Geophys. J. Int.* (2004) **157,** 441–454 doi: 10.1111/j.1365-246X.2004.02197.x

# Palaeosecular variation in Java and Bawean Islands (Indonesia) during the Brunhes chron

A. Elmaleh,[1,*] J.-P. Valet,[2] X. Quidelleur,[2,3] A. Solihin,[4] H. Bouquerel,[2] T. Tesson,[5] E. Mulyadi,[4] A. Khokhlov[6] and A. D. Wirakusumah[4]

[1] *Department of Earth Sciences, University of Cambridge, Downing Street, Cambridge* CB2 3EQ, *UK. E-mail: aelm03@esc.cam.ac.uk*
[2] *Laboratoire de Paléomagnétisme, IPGP,* 4 *Place Jussieu, case* 89, *Paris* F-75252, *Cedex* 5, *France*
[3] *Laboratoire de Géochronologie UPS—IPGP, Orsay, France*
[4] *Volcanological Survey of Indonesia, Bandung, Indonesia*
[5] *Merapi Volcano Observatory, Yogyakarta, Indonesia*
[6] *International Institute of Earthquake Prediction, Theory and Mathematical Geophysics, Moscow, Russia*

Accepted 2003 October 28. Received 2003 October 28; in original form 2003 March 4

## SUMMARY

A palaeomagnetic study has been conducted from Indonesian lava flows and dykes. Sampling was concentrated to the Merapi and Merbabu volcanoes (central Java), the Bromo–Tengger volcanic complex, the Lurus volcano (both east of Java), and the Bawean Island. Numerical dating indicates that the rock units sampled have ages that are well distributed within the Brunhes chron. Only a few reverse polarity flows were probably emplaced during the late Matuyama chron. Alternating field (AF) and thermal demagnetization treatments were routinely used for all sites. Results from both methods were generally in good agreement, demonstrating the reliability and the reproducibility of the palaeomagnetic determinations obtained from 36 independent sites. The large dispersion of the directions and the age distribution indicate that a large spectrum of the secular variation has been sampled. Our best estimate of the mean Brunhes field direction in Java is characterized by a zero declination and an inclination anomaly of $-4.7^\circ$ (with a 95 per cent confidence angle of $5.3^\circ$). This value agrees with an axial dipolar field model, or a model to which a persisting zonal quadrupolar term of a few per cent of the geocentric axial dipole is added. This study adds new constraints to recent results which suggested that a large zone of negative inclination anomalies may have persisted in the southwestern Pacific ocean over the past 500 Kyr, and possibly extended toward the eastern Indian ocean. The present results do not support such an extension. They also suggest that the inclination anomaly may have varied over 100 Kyr, and that it was more pronounced in recent times.

**Key words:** Brunhes chron, Indonesia, palaeosecular variation, volcanic rocks.

## 1 INTRODUCTION

Time-averaged geomagnetic field models indicate that the field geometry was mainly dipolar during the past 5 Myr (e.g. Schneider & Kent 1990). Several authors have also suggested that a small persistent axial quadrupole in the order of 5 per cent of $g_1^0$ provides the best fit to the data (e.g. Constable & Parker 1988; Schneider & Kent 1990; Quidelleur *et al.* 1994); Carlut & Courtillot 1998. The presence of other persisting non-axial dipolar terms is debated. Gubbins & Kelly (1993) noticed the persistence of northern high-latitude flux lobes in maps of the radial field ($B_r$) at the core–mantle boundary (CMB) (Gubbins & Kelly 1993) while Johnson & Constable (1997) and Johnson & Constable (1998) reported on the existence of anomalous $B_r$ at the CMB in the central Pacific ocean, linked to a large zone of inclination anomalies (defined as the observed palaeomagnetic inclination minus inclination predicted by a geocentric axial dipole). In Johnson & Constable (1997) (see their fig. 13(a)) model, this zone extends toward the eastern Indian ocean. Johnson & Constable (1998) suggest that this is a robust feature because the area has been extensively sampled, at least by Hawaiian lava flows and equatorial marine sediments. Elmaleh *et al.* (2001) recently compiled the available inclination data from the Pacific and eastern Indian oceans during the Brunhes chron and added new sedimentary records to improve the spatial coverage of sites. Their new map depicts large negative anomalies in the southwestern Pacific rather than in the central Pacific. The map also suggests a possible extension of negative anomalies toward the eastern Indian Ocean, but discrepancies between the existing records are observed.

The present study was aimed at documenting further the mean field in the eastern Indian ocean during the Brunhes chron from

*Formerly at IPGP, Paris, France.

records of Indonesian lava flows. The choice of the location was justified by the absence of data from Indonesia in recent palaeosecular-variation volcanic databases (Quidelleur *et al.* 1994; Johnson & Constable 1996). In addition, Indonesia is located within a whole longitudinal band largely devoid of Brunhes chron records from lava flows. Filling longitudinal gaps is important to investigate the existence of non-zonal terms. The equatorial position of the area is also appropriate to further constrain the possible persistence of a zonal quadrupole.

## 2 SITES AND SAMPLING

Java and the nearby small island of Bawean (Fig. 1a) are appropriate to study the Brunhes chron field for several reasons. Quaternary volcanism is widespread in Java, owing to intensive volcanism related to the subduction along the Java trench. A study of volcanic products of Bawean Island has shown that the island was built up during the Quaternary (Soeria-Atmadja *et al.* 1988; Bellon *et al.* 1990). Java and Bawean are part of the Sundaland block. Recent GPS studies have established that the Sundaland block is undeformed at the level of precision of the GPS measurements (Chamot-Rooke & Le Pichon 1999). Java and Bawean are not characterized by any large active faults, in contrast with Sumatra, which is crossed by a major strike-slip fault (the Great Sumatra fault). Therefore, we do not expect the palaeomagnetic measurements to be an indication of tectonic displacements, but rather a measure of palaeosecular variation.

During spring 2001, we sampled lava flows and dykes from the Merapi and Merbabu volcanoes (central Java), the Bromo–Tengger volcanic complex (east of Java), and the Lurus volcano (east of Java at the bank of Madura strait). We also sampled 14 lava flows and a dome on Bawean Island, located 150 km north of Surabaya in the Java sea (Fig. 1a). The choice of the sampling sites was guided by existing data on numerical ages and stratigraphy of the volcanic products.

We took 552 samples with a portable gasoline-powered drill and oriented them with a magnetic compass. Whenever possible, sun orientation was also measured. In this case, the true geographic azimuth could be calculated and used to orient the cores in the horizontal plane. The mean present day magnetic declinations for the Merapi–Merbabu, Bromo–Tengger, Lurus, and Bawean areas are $0.3 \pm 1.7^\circ$, $1.6 \pm 1.7^\circ$, $2.2 \pm 1.6^\circ$ and $0.9 \pm 1.2^\circ$, respectively. These values are in good agreement with the IGRF2000 (Mandea & Macmillan 2000) values ($1.0^\circ$, $1.3^\circ$, $1.4^\circ$ and $1.3^\circ$, respectively) and were used to correct the magnetic azimuth in the absence of sun orientation.

## 3 AGE CONTROL

### 3.1 Merapi and Merbabu

The sampling map of the Merapi–Merbabu area is shown in Fig. 1(c). The stratigraphic succession of the flows sampled at the Merapi and Merbabu volcanoes are shown in Figs 2(a) and (b). Most lava flows (Me01 to Me07) belong to the Batulawang pile (Bahar 1984; Newhall *et al.* 2000) and are part of Old Merapi according to the terminology of van Bemmelen (1949) (see also Bahar 1984; Wirakusumah *et al.* 1989; Newhall *et al.* 2000). This series forms the bulk of the eastern and northern slopes of Merapi. The oldest known deposit of the Old Merapi is the Sumbung (Cepogo) pyroclastic flow with a $^{14}$C age of $9630 \pm 60$ BP (Newhall *et al.* 2000). The lava flows that were sampled near Bakalan (Me07) and Deles (Me03, Me05 and Me04 in stratigraphic order) are among the oldest of the series. The oldest flow from what we called the Deles section (Me03) corresponds to the lowermost flow of the Bonjorejo series described by Berthommier (1990) and has a U-Th age of *ca* 6700 BP (see also Camus *et al.* 2000). This unit is cut by a fault mapped by the Volcanological Survey of Indonesia, that has not affected the overlying flow (Berthommier 1990). We sampled Me03 over a large area (*ca* 100 m). At Cepogo, we sampled two pyroxene-rich lava flows separated by flow rubble (Newhall *et al.* 2000). They are overlain by a pumiceous pyroclastic-flow deposit with a $2590 \pm 120$ BP charcoal level (Newhall *et al.* 2000). A major collapse separated the Old Merapi from the Young Merapi phases, as witnessed by the prominent somma rim of Merapi, which is open to the southwest (e.g. Wirakusumah *et al.* 1989). The age of this structure is a matter of debate. Newhall *et al.* (2000) suggested a $^{14}$C age of *ca* 1900 BP, based on dating of the youngest pyroclastic flow on the eastern side of Merapi. Several lava flows described by Wirakusumah *et al.* (1989) and Bahar (1984) erupted afterward, as the andesitic Kali Kuning flow (Me06).

There is no numerical dating of the Merbabu products. Nevertheless, Merbabu pyroclastic flows were found (Andreastuti *et al.* 2000) interbedded with Merapi products in the northern part of Merapi, within the narrow depression that separates Merapi from Merbabu. Therefore, both volcanoes have a common and recent period of activity. We therefore assume that the Mb01 to Mb04 Merbabu flows, which were sampled in two valleys at the foot of Jarak village in the depression that separates the two edifices, were deposited during the past 10 Kyr, although dating is still needed to confirm this interpretation.

### 3.2 Bromo–Tengger volcanic complex

A map of the sampled area and the stratigraphic succession of the sampled units and numerical dating available for the Bromo–Tengger products are presented in Figs 1(d) and 2(c). This stratigraphy is mainly based on studies by Zaennudin (1990), Mulyadi (1992) and Zaennudin *et al.* (1994). Samples were taken from the Ngadisari unit, the Old Tengger *sensu stricto* strato-volcano, and from Cemorolawang strato-volcano. The Ngadisari unit and Old Tengger *sensu stricto* belong to the Tengger volcano *sensu lato*, constituting the oldest part of the complex, were emplaced before the major Ngadisari caldera collapse event. Eruption of both units began before $822 \pm 90$ Ka, according to a K-Ar age from a flow crossed by the Sapikerep caldera collapse wall, the Pakel flow (Mulyadi 1992). The stratigraphic position of the nearby flow BT21, which belongs to the Ngadisari unit, could not be determined. Higher in the volcanic pile, and within the Old Tengger *sensu stricto* we sampled the BT07 and BT17-18 lava flows, which are separated by pyroclastic deposits. The BT07 flow is cut by three dykes (BT08, BT09 and BT19) which are oriented *ca* $110^\circ$N, and are interpreted as feeding dykes of the Ngadisari volcano (Mulyadi 1992; Zaennudin *et al.* 1994). The BT17-18 flow was sampled along the road leading to Mount Penanjakan. It is covered by a thick series of pyroclastic flows. Just below the summit of Mount Penanjakan, we sampled a series of five lava flows interbedded with pyroclastic flows (BT14 to BT10, in stratigraphic order) and two adjacent dykes (BT15 and BT16). The $152 \pm 30$ Ka upper age limit of the system was derived from K-Ar dating of the Sukapura ignimbrite, which is the pyroclastic product associated with the Ngadisari caldera collapse (Mulyadi 1992). Volcanic products that post-date this collapse, and belonging to the Cemorolawang strato-volcano, were sampled in the

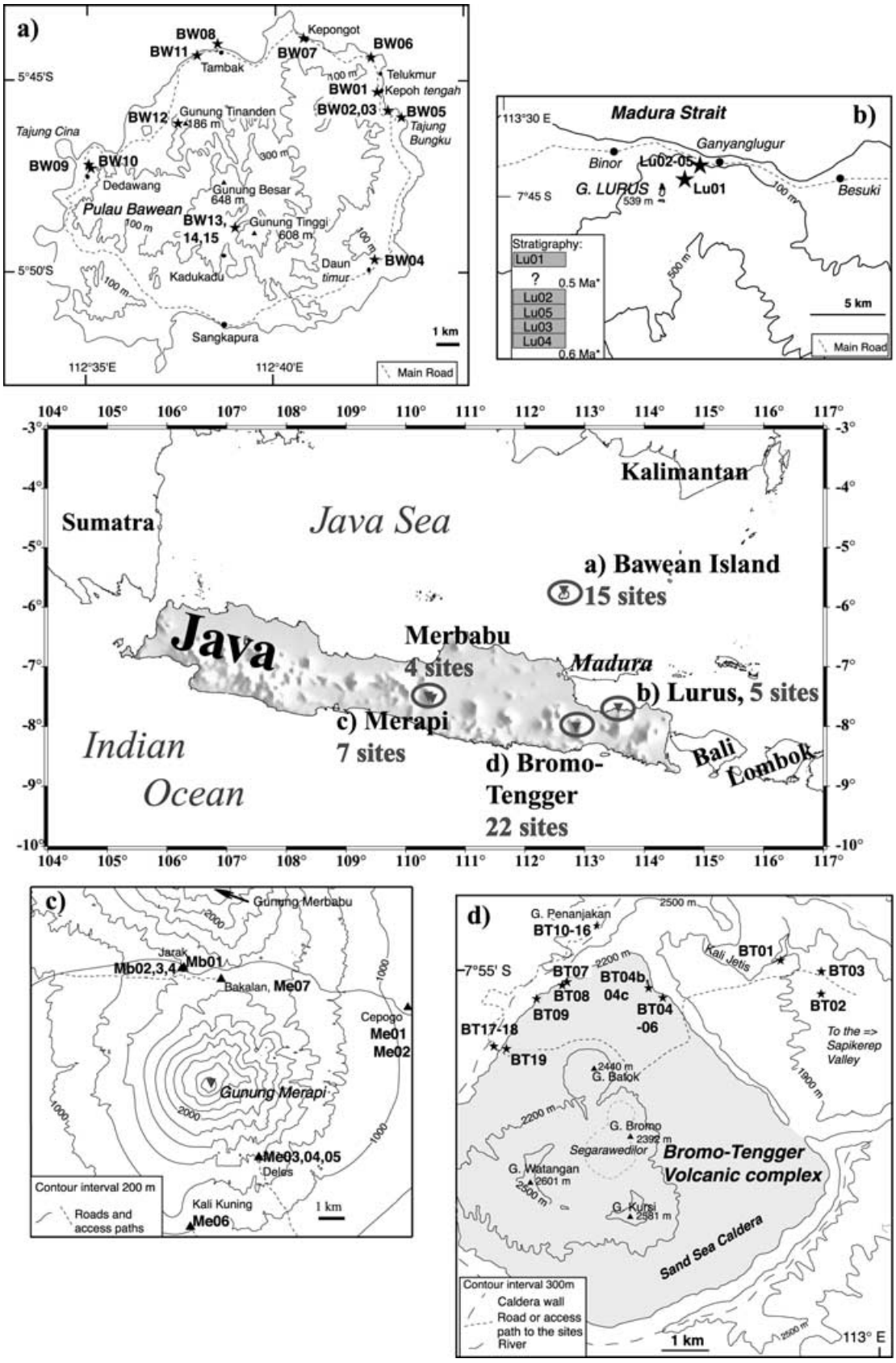


**Figure 1.** Map of locations sampled in Java and Bawean Islands, Indonesia. Topography is from ETOPO5. More detailed maps of Bawean Island, Lurus volcano, Merapi–Merbabu area and Bromo–Tengger volcanic complex with locations of sites sampled are shown in (a), (b), (c) and (d), respectively. The flows BT20 (7.92°S, 113.03°) and BT21 (7.89°S, 113.06°), taken further east in the Kali Jurang Ganten and Kali Kledung river beds respectively, are not shown on (d). The stratigraphy of the five lava flows sampled at the Lurus volcano is shown in (b).

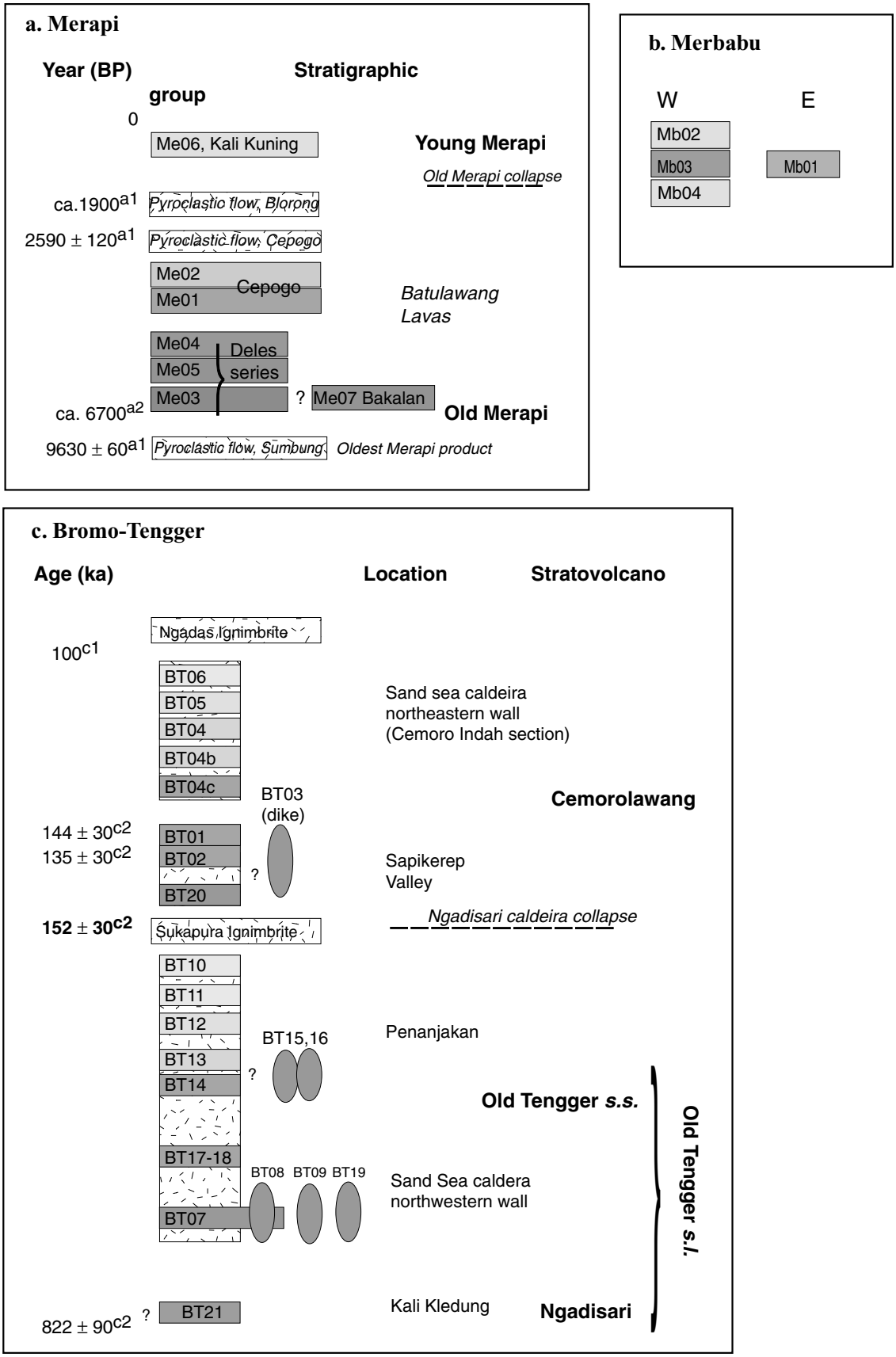


**Figure 2.** (a) to (c) show composite stratigraphy of the lava flows sampled at Merapi volcano, Merbabu volcano, and Bromo–Tengger volcanic complex respectively. a1: $^{14}C$ ages from Newhall *et al.* (2000), a2: U-Th disequilibrium age from Berthommier (1990), c1: K-Ar age, Zaennudin (1990), c2: K-Ar ages, Mulyadi (1992).

Sapikerep valley and in the Sand Sea caldera. The oldest flows of this phase were sampled in the Sapikerep valley. The lowest flow (BT20), which is surrounded by pyroclastic deposits, is overlain by the BT02 Ngadas andesitic lava flow and the BT01 big-feldspar lava flow (Mulyadi 1992; Zaennudin *et al.* 1994). K-Ar dating of BT01 and BT02 yielded identical ages of 135 ± 30 Ka for BT02, and 144 ± 30 Ka for BT01 (Mulyadi 1992; Zaennudin *et al.* 1994). Younger flows (BT04c, BT04b, BT04, BT05 and BT06 in stratigraphic order), which are interbedded with pyroclastic deposits, were sampled in the northeastern wall of the Sand Sea caldera. The *ca* 100 Ka age of one of the uppermost flows gives an upper age limit for the Cemorolawang series (Zaennudin 1990; Zaennudin *et al.* 1994). The stratigraphic position of the BT03 dyke, sampled near the Jetak cemetary, is unknown but its position in the Cemorolawang stratocone indicates that it is younger than *ca* 152 Ka.

### 3.3 Lurus

Lurus is an extinct leucite-bearing ultra-potassic volcano (Soeria-Atmadja *et al.* 1988). We sampled one flow uphill, presumably the highest in the stratigraphy, near Selo Banteng (Lu01). Four additional lava flows separated by flow rubble (Lu04, Lu03, Lu05, Lu02 in stratigraphic order) were sampled along the coastal road between Besuki and Binor (Fig. 1b). They belong to a section dated between 0.6 and 0.5 Ma (Soeria-Atmadja *et al.* 1988; Bellon *et al.* 1990).

### 3.4 Bawean Island

Volcanism of the Bawean Island is characterized by leucite-bearing, alkali ultra-potassic products, with an evolution leading to ultra-alkali phonolites (Soeria-Atmadja *et al.* 1988). Ages range from 0.3 to 0.8 Ma (Soeria-Atmadja *et al.* 1988; Bellon *et al.* 1990). We sampled 14 lava flows and a dome (BW12) around the island (Fig. 1a). Only four samples could be taken over a 1 m interval at BW03. This differs from our standard procedure which involved at least eight scattered samples per flow (the other exception is BT20, with five samples).

## 4 PALAEOMAGNETIC TECHNIQUES

All palaeomagnetic measurements were carried out in the shielded room of the Institut de Physique du Globe de Paris palaeomagnetic laboratory. Measurements were made using a JR5 spinner magnetometer. For each site, the natural remanent magnetization (NRM) of at least three samples was subjected to stepwise alternating field (AF) demagnetization from 5 mT up to 150 mT, using a three-axis coil system. A typical demagnetization sequence involved demagnetization steps of 5 mT between 5 and 50 mT, thereafter every 10 mT or 20 mT up to 100 mT and above if necessary. At least three samples per site were subjected to thermal treatment (except Lu05, Me06, and BW01 where only two samples were thermally demagnetized) including at least 11 steps, up to 590 °C or 610 °C. Low-field magnetic susceptibility was measured at room temperature using either a MS2 (Bartington Ltd, UK) or a Minisep (Molspin Ltd, UK) magnetic susceptibility instrument, after each heating step. In some cases, the susceptibility indicated possible mineralogical changes induced by heating. The fact that identical directions were obtained using AF and thermal treatments indicates that the direction of the ChRM was not affected by these mineralogical changes, which was expected because of the low residual field measured in the furnace (less than 20 nT), which is encased in a $\mu$-metal shield.

The directions of the characteristic remanent magnetization (ChRM) were determined using principal component analysis on data from 6 to 10 demagnetization steps (Kirschvink 1980). The $\alpha_{95}$ about the principal direction never exceeded 2.5°. The final data set includes only samples with Zijderveld (1967) diagrams characterized by a linear decay of the vector through the origin of the plot. Site mean directions (Table 1) were calculated using Fisher (1953) statistics for flows with specimens from at least four samples (seven on average). Among the samples that were not taken into account in this calculation, first, most did not satisfy the criteria defined above, and secondly, a few samples with good demagnetization diagrams were discarded because they showed strongly discrepant directions with respect to other samples, probably resulting from disorientation. In a few cases, samples from the first category showed evidence for an isothermal remanent magnetization (IRM) possibly acquired via a lightning strike. Finally, when two specimens from the same core were demagnetized using a different technique (either thermally or by AF methods), we included both in the average.

## 5 DEMAGNETIZATION CHARACTERISTICS

Samples from 53 sites have been measured and stepwise demagnetized. Reverse polarity directions were obtained for three flows (BW09, BW10 and BW13), which is consistent with the maximum age of *ca* 0.8 Ma measured at Bawean (Soeria-Atmadja *et al.* 1988; Bellon *et al.* 1990). These flows will not be considered further in this study of the Brunhes field. Five sites (BW11, BW14, BW15 and Lu01) were characterized by low quality demagnetization diagrams for nearly all samples and were discarded.

We identified three main types of behaviour upon stepwise thermal demagnetization (Fig. 3a). Type 1 samples have a wide spectrum of unblocking temperatures ending at the Curie temperature of magnetite (580 °C), which indicates that the magnetization is carried by magnetite with variable grain sizes and/or variable titanium content. The type 2 samples are characterized by a narrow range of unblocking temperatures (around 580 °C), which is characteristic of fine-grained magnetite. The type 3 samples (which represent about a third of the 164 samples that were thermally demagnetized, and with a preponderance from the Bromo–Tengger volcanic complex) are characterized by a two-step decay of the magnetic moment with temperature. Only site BW01, the case of which will be discussed below, does not fit in any of these categories.

Typical demagnetization diagrams obtained after thermal or AF treatment of samples from several sites are shown in Figs 3(b) and 4. All type 2 samples exhibit a linear decay of the vector toward the origin of the vector component plot after removal of a low temperature component, as in the two examples in Fig. 3(b). Because of its random character, this low temperature component is probably a viscous component acquired during storage. The type 1 and 3 samples frequently exhibit another secondary component. Its origin can in some cases be attributed to a viscous component acquired in the present-day field (as in Lu02-02, Fig. 3b) but there are many exceptions to this behaviour. Two particular cases can be emphasized. First, all samples from BT07 were characterized by a secondary component that was removed between 120 and 250 °C or at 5–15 mT and with a direction close to that of dyke BT08, which cuts flow BT07. This overprint was therefore interpreted as a partial thermoremanent magnetization caused by reheating. All samples from BT04b carry a secondary component with variable directions

**Table 1.** Palaeomagnetic directions for the Java and Bawean Islands lavas.

| Site | Data used | $n/N$ | $D$ (°) | $I$ (°) | $\kappa$ | $\alpha_{95}$ (°) | $\lambda$ (°) | $\phi$ (°) | Type |
|---|---|---|---|---|---|---|---|---|---|
| *Merbabu* | | | | | | | | | |
| Mb01 | AF+TH | 6/11 | 14.5 | −14.1 | 106.3 | 6.5 | | | 1,2 |
| Mb02 | AF+TH | 6/8 | 3.6 | −33.5 | 436.3 | 3.2 | 78.6 | 272.8 | 1 |
| Mb03* | AF+TH | 7/8 | 9.6 | −15.6 | 499.7 | 2.7 | | | 1 |
| *Mb01+Mb03* | AF+TH | 13/19 | 10.5 | −14.9 | 193.7 | 3.0 | 79.6 | 201.6 | |
| Mb04* | AF+TH | 5/10 | 1.1 | −1.9 | 197.1 | 5.5 | 83.4 | 120 | 1 |
| *Merapi* | | | | | | | | | |
| Me01• | AF+TH | 5/7 | 1.8 | −30.4 | 424.1 | 3.7 | | | 1,2 |
| Me02 | AF+TH | 6/6 | 2.0 | −26.7 | 634.9 | 2.7 | | | 1,2 |
| *Me01+Me02* | AF+TH | 11/12 | 1.9 | −28.4 | 900 | 2.2 | 82.2 | 276.9 | |
| Me03[1] | AF+TH | 8/8 | 352.2 | −30.9 | 404.7 | 2.8 | 78.1 | 329.7 | 2 |
| Me04[1] | AF+TH | 7/10 | 350.5 | −28.1 | 443.7 | 2.9 | 78.1 | 341.2 | 3 |
| Me05•[,3] | AF+TH | 9/10 | 0.8 | −28.4 | 173.0 | 3.9 | 82.4 | 284.6 | 2 |
| Me06 | AF | 7/9 | 354.9 | −33.4 | 462.5 | 2.8 | 78.2 | 314.9 | 1,2 |
| Me07*[,1] | AF+TH | 8/12 | 353.7 | −4.4 | 228.0 | 3.7 | 81.8 | 60.3 | 1,2 |
| *Bromo-Tengger* | | | | | | | | | |
| BT01 | AF+TH | 6/7 | 7.2 | −11.1 | 1086.7 | 2.0 | 82.5 | 185.5 | 1 |
| BT02* | AF+TH | 7/10 | 355.8 | −10.1 | 839.8 | 2.1 | 85 | 56.9 | 1 |
| BT03[1] | AF+TH | 9/10 | 10.8 | −46.0 | 144.5 | 4.3 | 68 | 266.6 | 3 |
| BT04* | AF+TH | 6/9 | 4.2 | −31.4 | 183.0 | 5.0 | 80.1 | 269.0 | 1,3 |
| BT04b* | AF+TH | 5/10 | 10.5 | 3.9 | 125.7 | 6.8 | 75.6 | 160.1 | 1,3 |
| BT04c* | AF+TH | 6/11 | 354.8 | −28.3 | 821.6 | 2.3 | 81.2 | 328.0 | 1 |
| BT05[1] | AF+TH | 8/10 | 4.8 | −3.1 | 259.0 | 3.4 | 82 | 150.1 | 3 |
| BT06[1] | AF+TH | 5/11 | 23.5 | −44.8 | 14.5 | 6.4 | 61 | 245.5 | 1,3 |
| BT07 | AF+TH | 5/9 | 343.9 | 7.4 | 149.0 | 6.3 | 70.2 | 58.3 | 1,2 |
| BT08[1] | AF+TH | 8/8 | 354.7 | −19.6 | 341.2 | 3.0 | 84.3 | 360.0 | 3 |
| BT09 | AF+TH | 10/11 | 353.1 | −26.5 | 313.9 | 2.7 | 80.9 | 340.4 | 1,2,3 |
| BT11* | AF | 5/8 | 352.1 | −10.2 | 283.6 | 4.6 | 81.7 | 41.8 | 1 |
| BT12 | AF+TH | 5/8 | 335.9 | −6.0 | 275.2 | 4.6 | 65.5 | 33.1 | 1,3 |
| BT13[1,*] | AF | 5/10 | 350.9 | −26.7 | 126.5 | 6.8 | 79.1 | 347.3 | 3 |
| BT14* | AF | 4/9 | 0.5 | −23.7 | 586.2 | 3.8 | 85.5 | 286.7 | 3 |
| BT15[1] | AF+TH | 7/9 | 336.4 | −12.9 | 209.8 | 4.2 | | | 1,2 |
| BT16 | AF+TH | 5/10 | 339.1 | −12.5 | 164.3 | 6.0 | | | 3 |
| *BT15+BT16* | AF+TH | 12/19 | 337.5 | −12.7 | 196.1 | 3.1 | 67.6 | 25.3 | |
| BT17-18[1,*] | AF+TH | 6/14 | 11.8 | −35.9 | 104.1 | 6.6 | 73.5 | 250.5 | 3 |
| BT19 | AF+TH | 8/9 | 354.0 | −10.8 | 94.2 | 5.7 | 83.5 | 45.1 | 1,2 |
| BT20[2] | AF+TH | 6/8 | 19.5 | −35.7 | 128.5 | 5.9 | 67.7 | 237.1 | 3 |
| BT21[2] | AF+TH | 9/10 | 2.7 | −8.8 | 150.5 | 4.2 | 85.6 | 151.0 | 3 |
| *Lurus* | | | | | | | | | |
| Lu02 | AF+TH | 9/10 | 6.9 | −19.1 | 493.1 | 2.3 | | | 1,2 |
| Lu03 | AF+TH | 8/8 | 6.8 | −20.8 | 253.2 | 3.5 | | | 1,2 |
| Lu04 | AF+TH | 8/8 | 4.3 | −20.9 | 169.5 | 4.3 | | | 1,2 |
| Lu05 | AF+TH | 5/6 | 7.3 | −20.0 | 232.2 | 5.0 | | | 2 |
| Lurus | AF+TH | 30/32 | 6.3 | −20.2 | 261.4 | 1.6 | 83.2 | 227.6 | |
| *Pulau Bawean* | | | | | | | | | |
| BW01 | AF | 6/8 | 11.7 | −33.8 | 123.7 | 6.0 | 72.9 | 251.9 | |
| BW02[1] | AF+TH | 8/8 | 342.3 | −5.7 | 312.3 | 3.1 | 72.1 | 31.3 | 1,2 |
| BW03 | AF+TH | 4/4 | 1.3 | 15.3 | 509.0 | 4.1 | 76.4 | 118.2 | 2 |
| BW04 | AF+TH | 8/9 | 6.9 | −21.2 | 96.1 | 5.7 | 81.5 | 240.2 | 2 |
| BW06[1] | AF+TH | 10/10 | 14.6 | 4.1 | 274.0 | 2.9 | 73.5 | 175 | 1,3 |
| BW07 | AF+TH | 11/11 | 16.4 | −24.9 | 593.1 | 1.9 | 72.2 | 228.3 | 2 |
| BW08 | AF+TH | 8/9 | 3.4 | 3.7 | 132.1 | 4.8 | 81.7 | 136.9 | 1 |

Site: the superscripted number that follows the site name indicates how many pairs of specimens from a single sample were thermally or AF demagnetized; in italics: sites merged together (see Table 2); about the discarded samples: no symbol is drawn for samples discarded because the demagnetization diagram does not satisfy the requirements defined in the text; other cases: • are probably disoriented samples; *: samples that do not satisfy the requirements and that are suspected of having been struck by lightning; data used: to calculate a mean direction [alternating field (AF) or thermal (TH) treatment]; n: number of directions used for calculating the mean; $N$: number of samples treated; $D$: declination; $I$: inclination; $\kappa$; dispersion parameter and $\alpha_{95}$: radius of the 95 per cent confidence cone (from Fisher (1953) statistics); $\lambda$ and $\phi$: VGP latitude and longitude for the final site mean direction (sites merged: see Table 2); type: of behaviour upon thermal demagnetization (refers to Fig. 3).

(between $D = 50°$, $I = 30°$ and $D = 7°$, $I = -14°$) and strong intensities (from 6 to 58 A m$^{-1}$), which was interpreted as an IRM acquired by lightning. In the latter case, a stable remanent component could be isolated for half of the samples and gave consistent directions that are therefore interpreted as ChRM directions for this site.

No ChRM components could be isolated by thermal demagnetization for several sites. This includes samples from Me06 with

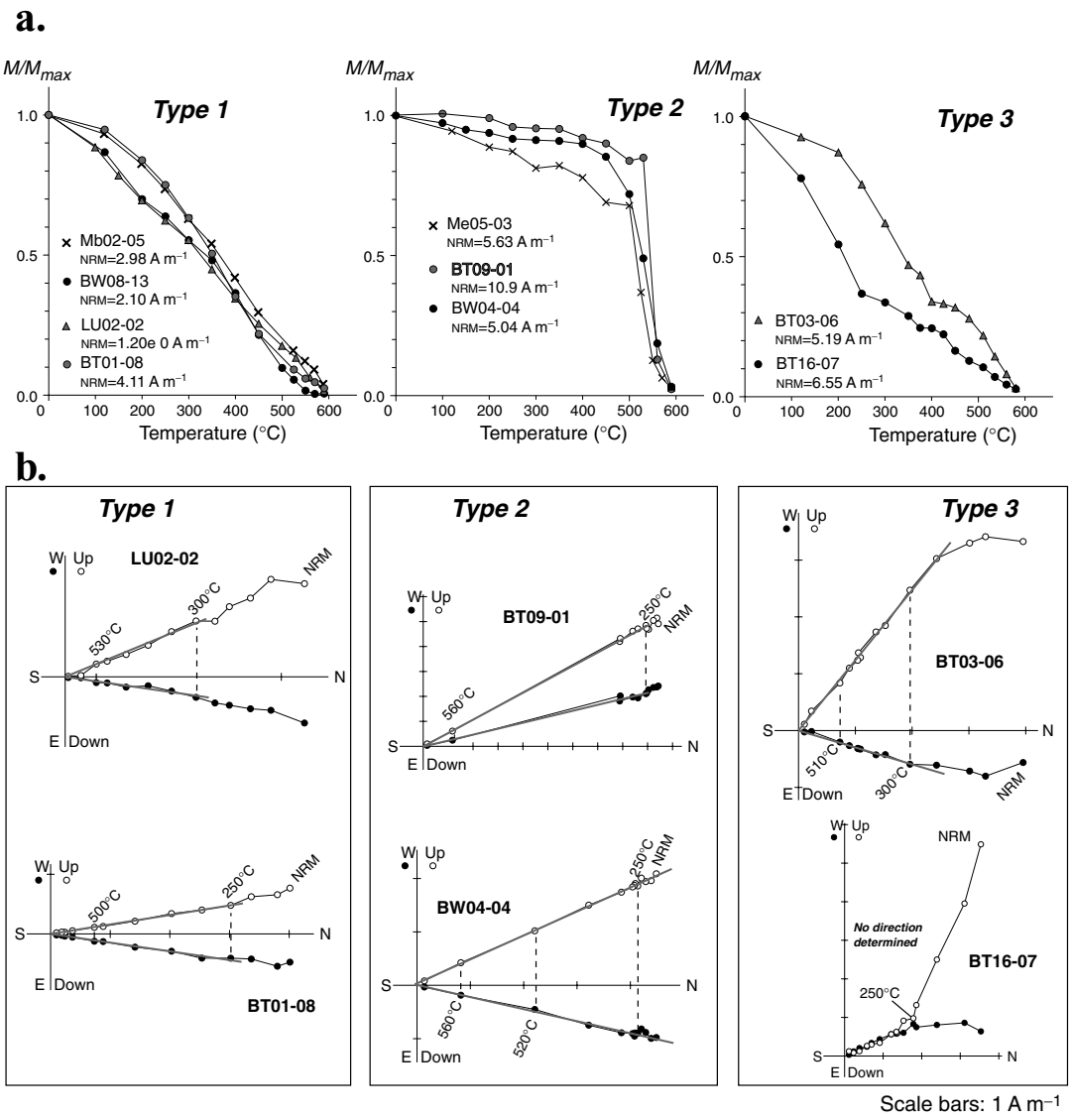


**Figure 3.** (a) Typical examples of thermal demagnetization curves. As in all the following figures, the name of the samples is composed first of the site name (e.g. BT03), with the number following the hyphen indicating the sample number (−06). The magnetic moment is normalized to the maximum value. Three types of behaviour are distinguished: (i) A regular decrease of the moment across a wide unblocking temperature interval, that ends at the Curie temperature of magnetite. (ii) A much more narrow range of unblocking temperatures, with most of the unblocking occurring near the Curie temperature of magnetite. (iii) Decay of the moment across two temperature steps. (b) Examples of Zijderveld diagrams corresponding to some of the thermal demagnetization curves shown in (a). The convention for Zijderveld diagrams (as in all following figures) is: solid symbols correspond to projections onto the horizontal plane, while open symbols represent projections onto the vertical plane. Lines indicate fits to the ChRM vector by principal component analysis. Calculations and plots were made using the PaleoMac software (Cogné 2003).

noisy thermal demagnetization curves, samples from site BW01 and samples from sites BT11, BT13 and BT14. Most of the BW01 samples are characterized by a low coercivity (0–15 mT) and mid-temperature (up to 400 °C) secondary component parallel to the drilling (Fig. 4), indicating that this component is likely to be a drilling-induced remanent magnetization (DIRM) (e.g. Audunsson & Levi 1989; Genevey *et al.* 2002). In that case, as for many samples from the other sites quoted, AF demagnetization was able to isolate a stable component of a presumably primary origin (e.g. BT13-09 in Fig. 4) so that site average directions could be calculated.

In most cases, when two specimens from a given core were successfully demagnetized, one with AF and the other by thermal treatment, they yielded identical mean directions ±4° or less (as in the case of site Me04, in Fig. 4). However, for site BT21, the two techniques yielded discrepant directions that differ by 6° (BT21-10) and by 11° (BT21-08). Since site mean directions calculated using either thermal or AF results are in good agreement within the 95 per cent confidence interval (Table 1), we did not discarded this site.

In Fig. 5(a), we compare the mean directions obtained after AF demagnetization with those derived from thermal demagnetization, with roughly the same number of samples in both cases (see Table 1). Note that Mb01 and Mb03 have been treated together (see below). The mean directions of the subsets of results obtained after either thermal or AF demagnetization are statistically identical (Fig. 5a). Since this comparison cannot be achieved for all sites, we also compared the mean directions obtained by one technique with the site mean direction. This is shown in Figs 5(b) and (c), where the inclinations and the declinations are separately plotted. In each

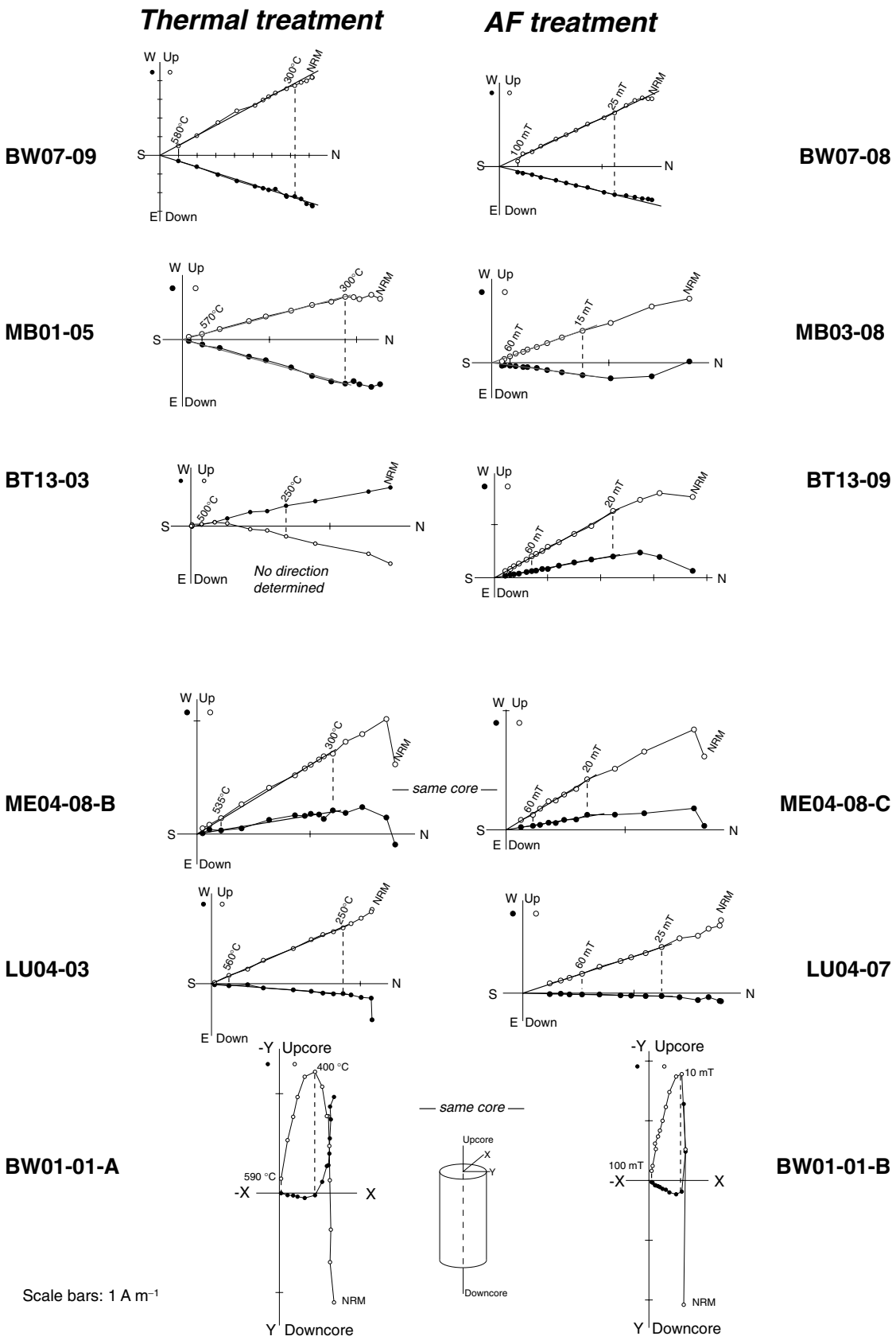


**Figure 4.** Examples of Zijderveld diagrams from each of the volcanoes or volcanic complexes sampled: (a) thermal demagnetization diagrams, (b) AF demagnetization diagrams. Conventions for the diagrams are as in Fig. 3. No ChRM was determined for BT13-03. The Zijderveld diagrams for the two samples from site BW01, in core coordinates, show evidence for a drilling-induced overprint that is easily removed by AF treatment, while it is more difficult to isolate using thermal treatment.

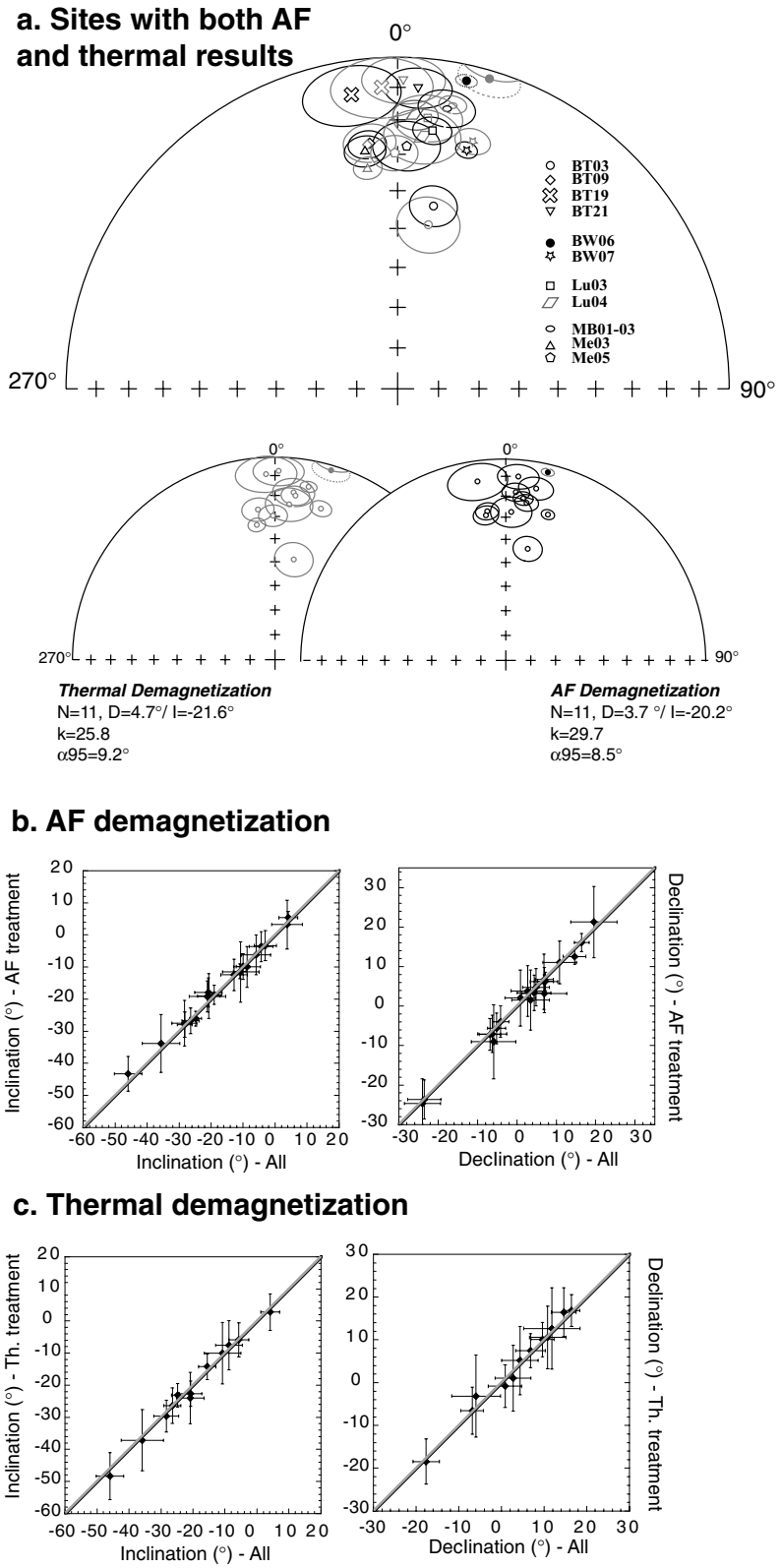


**Figure 5.** (a) Equal area projections of site means calculated with either only AF results (black) or thermal results (gray), using Fisher statistics. Open symbols : upper hemisphere; solid symbols: lower hemisphere projection. 95 per cent confidence cones are drawn. Upper stereo-plot: one site corresponds to each symbol; the key is given in the right-hand side of the figure. Lower stereo-plots: data separated according to either treatment and statistical parameters. (b) Comparison of site mean inclinations and declinations from Fisher statistics either on all the specimens for a given site (abscissas), or only (b) on AF demagnetized or (c) thermally demagnetized specimens. The 1:1 line, corresponding to identical results for the whole site, and the AF or thermal demagnetization results is shown as a gray line. Fisherian 95 per cent confidence intervals are plotted as error bars.

**Table 2.** Angular distance between the mean directions of successive flows or nearby dykes.

| Successive flows or dyke family | $\Sigma\alpha_{95}$ | Vector Angle | Difference |
|---|---|---|---|
| *Mb01/Mb03* | *9.2* | *5* | <0 |
| *Me01/Me02* | *6.4* | *3.7* | <0 |
| Me03/Me05 | 6.7 | 7.8 | >0 |
| Me05/Me04 | 6.8 | 9.0 | >0 |
| BT01/BT02 | 4.1 | 11.3 | >0 |
| *BT15/BT16* | *10.2* | *2.7* | <0 |
| BT09/BT08 | 5.7 | 7.1 | >0 |
| BT09/BT19 | 8.4 | 15.7 | >0 |
| BT19/BT08 | 8.7 | 8.8 | ∼0 |
| *Lu04/Lu03-05* | *6.8* | *2.3* | <0 |
| *Lu03-05/Lu02* | *4.8* | *1.3* | <0 |

Successive flows: as observed on the field (Mb01 and Mb03 are in fact nearby flows); dyke family: sharing a similar orientation (see also Mulyadi 1992); $\Sigma\ \alpha_{95}$: sum of $\alpha_{95}$ for the two flows; vector angle: between the mean directions of the two flows or dykes; difference: between the last two parameters.
Merged flows in italic.

plot, the directions calculated for AF (Fig. 5b) or thermal (Fig. 5c) demagnetization are compared to the corresponding site mean directions. Satisfactory agreement is always achieved within the error bars.

## 6 SITE MEAN DIRECTIONS

A mean palaeomagnetic direction for the Brunhes chron, as recorded in lava flows from Java and Bawean, was determined from 43 Brunhes age sites (Table 1). Only three sites (BT10, BW05 and BW12, a phonolite dome emplaced and growing at low temperature) were excluded because scatter of the directions did not allow us to calculate a site mean direction. It can be noted that all Virtual Geomagnetic Pole (VGP) latitudes are $\geq 60^\circ$ (Table 1). Therefore, none of the data can be considered as transitional.

In the absence of systematic dating, we checked whether successive flows were characterized by statistically identical directions, which would suggest that they were associated with eruptions that occurred over a short period of time. It is clear in Table 1 that successive flows Mb02, Mb03 and Mb04 have statistically different directions, whereas Mb01 and Mb03 (which were sampled in two parallel rivers) have identical directions, as shown in Table 2. The Me01 and Me02 Merapi flows, all the Lurus flows, and BT15 and BT16 dykes have overlapping 95 per cent confidence intervals. Moreover, the flows were only separated by flow rubble, and no baked soil was noticed. Therefore, they should be considered as single units (Table 2). After averaging all directions within each unit, we obtained 37 independent records of the Brunhes field (Table 1).

The sites lie within a *ca* 270–350 km rectangle and are close enough to each other to be treated as a single geographical area. The difference of 2.2° in latitude between the northernmost and the southernmost sites implies that the expected geocentric axial dipole (GAD) inclination goes from $-11.3^\circ$ to $-15.6^\circ$. One approach would be to calculate common latitude directions, by transforming the inclinations as if each site were taken at the same latitude. However, this would distort the actual distribution of site mean directions. Therefore, in order to obtain a representative inclination anomaly, we will consider a latitude calculated as the mean of the individual latitudes (7.4°S) if all Brunhes age sites are considered.

If one calculates the mean direction for the 37 Brunhes sites, the maximum angular distance with respect to this mean is 33.7° for BW03. This site is a small dyke with only four samples. Therefore, we will not consider this site any further, which now leaves 36 Brunhes age sites. The site mean direction for flow Me03 is very well constrained ($\alpha_{95} = 2.8^\circ$) and does not differ much from that of nearby flows. Therefore, we decided not to discard it. The mean directions of all 36 independent sites are plotted in Fig. 6. Most data are clustered about the mean direction of all sites (open star), but 11 sites lie outside a cone of 20° about this mean direction. One may wonder to what extent the present distribution of site mean directions is related to the timing of successive eruptions. The distributions of the mean directions obtained for the Bromo–Tengger, Bawean and the Merapi–Merbabu area are shown in Fig. 7. We note that the directions from sequences of lavas (e.g. the Cemoro Indah section) or from the Ngadisari dyke family are scattered over

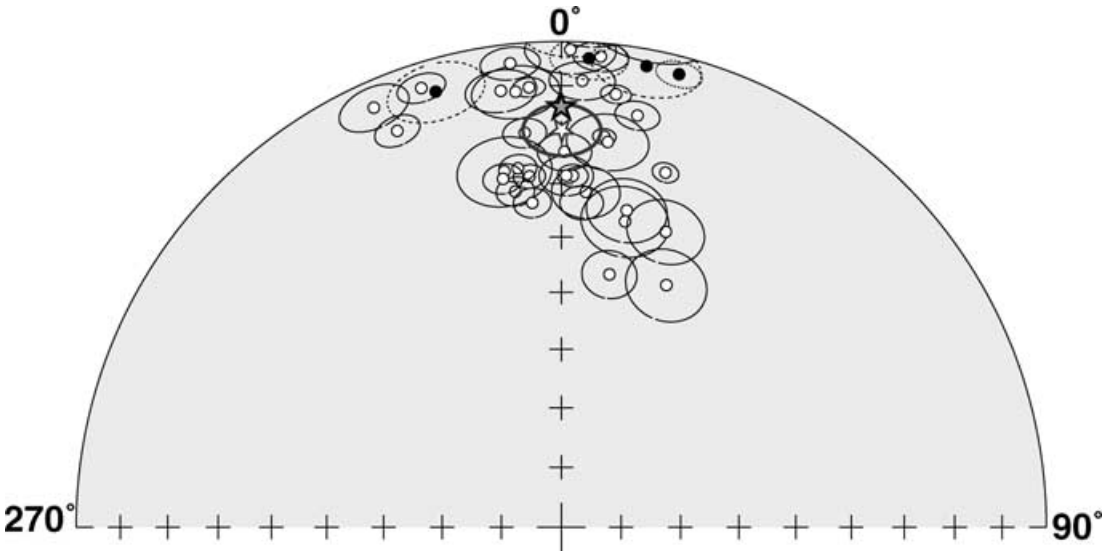


**Figure 6.** Equal area projection of the mean palaeomagnetic directions for the 36 independent Brunhes age flows (Table 1, see text for explanation). Conventions as is Fig. 5. The dipole value corresponding to the site mean latitude is plotted as a solid star (although the inclination is negative), and the site mean direction is plotted as an open star, with confidence interval shown at 95 per cent.

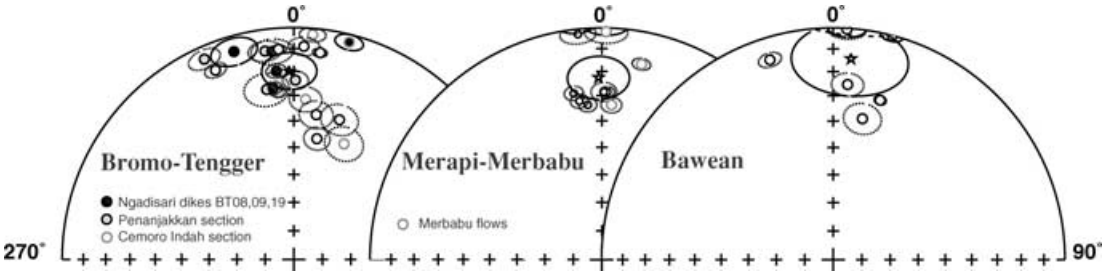


**Figure 7.** Site mean directions for the three volcanic groups Bromo–Tengger, Merapi–Merbabu and Bawean. Sites from a given section or those belonging to a family of dykes share the same pattern. Mean directions are plotted as stars, and Fisherian 95 per cent confidence intervals are drawn.

**Table 3.** Mean directions for several subsets of the lava flows and dykes from Java and Bawean Islands.

| Sub set | $N$ | $D$ (°) | $I$ (°) | $\kappa$ | $\alpha_{95}$ (°) | VGP scatter (°) | $\sigma$D (°) | $\sigma\ I$ (°) | Mean Lat. S (°) | $\Delta I$ (°) |
|---|---|---|---|---|---|---|---|---|---|---|
| Brunhes | 36 | 0.1 | −19.3 | 21.1 | 5.3 | 13.9 | 11.2 | 14.4 | 7.4 | −4.7 |
| Age 0–10 Ka[1] | 9 | 358.9 | −22.8 | 35.2 | 8.8 | 10.5 | 6.4 | 12.3 | 7.5 | −8.0 |
| Age 100–150 Ka[2] | 9 | 7.2 | −23.2 | 16.3 | 13.1 | 17.1 | 9.6 | 18.3 | 7.9 | −7.7 |
| Age <150 Ka[3] | 18 | 3.0 | −23.1 | 22.5 | 7.5 | 13.8 | 9.5 | 15.2 | 7.7 | −8.0 |
| Age >150 Ka[4] | 18 | 357.4 | −15.4 | 21.5 | 7.6 | 14.4 | 12.4 | 12.5 | 7.1 | −1.4 |

Sub-set: according to the age; $N$: number of sites used; $D$: declination, $I$: inclination; $\kappa$: dispersion parameter; $\alpha_{95}$: confidence angle (from Fisher (1953) statistics); VGP scatter: standard deviation of the distribution of angles between the VGPs and the geographic pole; $\sigma D$ and $\sigma I$: standard deviation of the distributions of declinations and inclinations, respectively; mean lat.: mean latitude calculated for the N sites considered; $\Delta I$: inclination anomaly.
[1]: corresponds to Merapi–Merbabu, [2]: Cemoro Indah section and Sapikerep valley sites, [3]: [1] + [2], [4]: remaining Brunhes age sites.

a large portion of the stereo-plot. Therefore, there is no evidence that short time intervals would have been repeatedly sampled. Note that this large scatter observed within single sections also rules out the possibility of tectonic rotations or block tilting to account for the present distribution. Therefore, we consider that the distribution of the directions reflect a random sampling of the palaeosecular variation.

## 7 DISCUSSION: BRUNHES MEAN FIELD DIRECTION

### 7.1 Robustness of the mean field direction

The final Brunhes mean direction is characterized by a mean inclination of $-19.3^\circ$ and a mean declination of $0.1^\circ$($n = 36$, $\alpha_{95} = 5.3^\circ$, $k = 21.1$) (Table 3). Given the scatter of the data, we have tested the robustness of this result. If we remove sites with an angular distance from the site mean direction that exceeds 25° (which leaves 31 directions), the averaged direction does not change significantly ($I = -19.5^\circ$, $D = 0.2^\circ$, $\alpha_{95} = 4.9^\circ$, $\kappa = 29.2$). Keeping only sites with angular distance $\geq 20^\circ$ (25 sites) yields $I = -20.7^\circ$, $D = 0.2^\circ$ ($\alpha_{95} = 4.4^\circ$, $\kappa = 43.7$). Similarly, keeping only the 28 sites with $\alpha_{95}$ lesser or equal to 5° yields $I = -18.1^\circ$, $D = 359.4^\circ$ ($\alpha_{95} = 5.6^\circ$, $\kappa = 24.5$). The robustness of the mean direction has also been tested using a jackknife approach. The resulting variations are always small, with mean declinations ranging from $-0.4^\circ$ to 0.9° and mean inclinations from $-20^\circ$ to $-18.5^\circ$. The VGP scatter (calculated as the angular dispersion with respect to the Earth's rotation axis) is 13.9°. As can be seen in Fig. 8, this value is in close agreement with the mean value at this latitude extracted from the Quidelleur *et al.* (1994) database (*ca* 14°). Recall that almost no data from the longitude band of Indonesia were present in the data set considered. Similarly, declination and inclination scatter values are close to the values from the Quidelleur *et al.* (1994) database (10 and 14°, respectively). This provides a good indication that the palaeosecular variation has been satisfactorily sampled.

The mean Brunhes field direction is characterized by a mean inclination anomaly of $-4.7 \pm 5.3^\circ$ and an almost null declination. One of the objectives of this study was to constrain the western extension of the zone of negative inclination anomalies observed from southwestern Pacific sediments studied by Elmaleh *et al.* (2001). Our new results do not support such an extension.

The mean field direction inferred from the sites mean direction is consistent with a purely dipolar field model, but also with a dipolar field model in which a zonal quadrupole contributes 5 per cent of $g_1^0$ (in that case, $\Delta I = -4^\circ$). It is interesting to note that this site follows the general trend toward negative inclination anomalies that characterizes most sedimentary or volcanic databases for the past few million years (Schneider & Kent 1990; Quidelleur *et al.* 1994). This feature was adequately described, in most cases, by the persistence of a zonal quadrupole of about 5 per cent of the geocentric axial dipole. However, the 95 per cent confidence interval also includes a dipolar mean field direction (Fig. 6). The present distribution is somehow distorted compared to a Fisher distribution. Therefore, one has to be very careful as to interpreting both the mean direction and the $\alpha_{95}$ value. Khokhlov *et al.* (2001) have shown that a set of independent and instantaneous field directions, as can be inferred from palaeomagnetic measurements on time-independent lava flows, should not necessarily be Fisher distributed if the field can be described as a giant Gaussian process, as first suggested by Constable & Parker (1988). Following Khokhlov *et al.* (2001), it is possible to evaluate the ability of different statistical models to describe the present data set, without distorting the distribution via the Fisher statistics, which may not be appropriate in the present case. The issue is not to choose between the several statistical field models, but to check whether, in the frame of such models, the whole data set is better fitted by a model in which the mean field is purely geocentric axial dipolar or includes

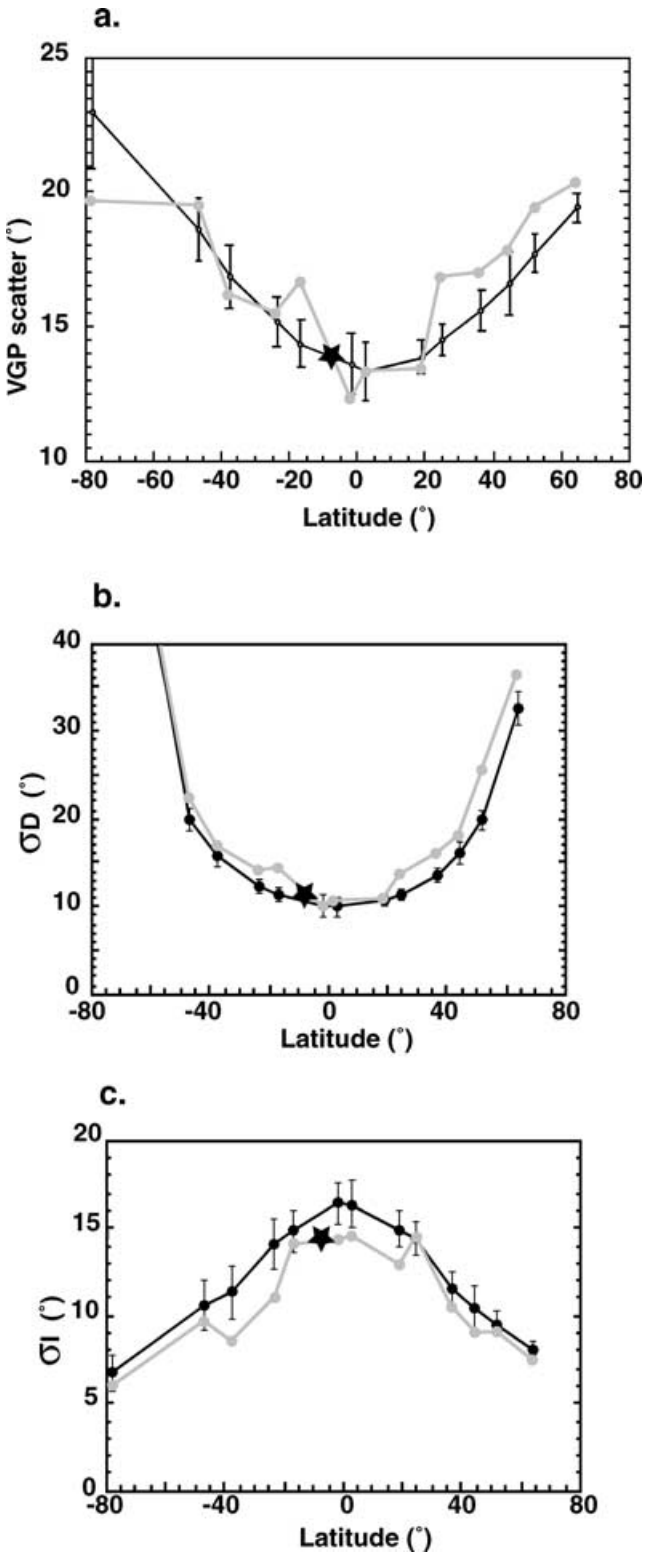


**Figure 8.** Dispersion parameters obtained for the 36 independent Brunhes directions (black stars, see Table 3) plotted together with the data from the Quidelleur *et al.* (1994) 0–5 Myr database (gray) and the predictions of the C1 statistical model of Quidelleur & Courtillot (1996) with errors (black). Redrawn after Quidelleur & Courtillot (1996). (a) Angular dispersion of virtual geomagnetic poles (VGP) with respect to the Earth' rotation axis. (b) Standard deviation of the distribution of declination. (c) Standard deviation of the distribution of inclination.

a small quadrupolar term. It is now well established that the pioneer model proposed by Constable & Parker (1988) provides a poor fit to the VGP scatter data (Quidelleur & Courtillot 1996; Constable & Johnson 1999). The model C1 proposed by Quidelleur & Courtillot (1996) and the model CJ98 (Constable & Johnson 1999), showing better performances with respect to that point, were tested using the formalism developed by Khokhlov *et al.* (2001) as well as derived models with a zero mean quadrupolar term (C1-0 and CJ98-0 respectively). The results of the $\chi^2$ and Kolmogorov–Smirnov (KS) tests (see Khokhlov *et al.* 2001, for explanation), show that adding a non-zero mean quadrupolar term does not improve the fit to the data, which is satisfactory in almost all cases (Table 4, Fig. 9). However, results of the $\chi 2$ test suggests that there is a 90 per cent probability of rejecting the CJ98 model. This observation would suggest that, as far as the Constable & Johnson (1999) model is concerned, adding a non-zero mean quadrupolar term is even worse, but conclusions are more shaded when considering the KS tests results. Moreover, this conclusion does not hold true for the Quidelleur & Courtillot (1996) model. The model CJ98-0 provides the best results, as already observed by Khokhlov *et al.* (2001) for the Brunhes database. It will be interesting from that point of view to integrate our new data with the whole database. Concerning our primary objective, we can conclude that, in the frame of statistical models, it is not necessary to add a persistent quadrupolar term to fit our data.

### 7.2 Time variations

The time distribution of the sites allows us to examine a possible temporal evolution of the field by comparing the mean directions of subsets of different ages. The recent 0–150 Ka period (Fig. 10) is characterized by a mean inclination anomaly of $-8 \pm 7.5^\circ$ (calculated with an appropriate mean latitude, see Table 3). The fact that the 0–10 and 100–150 Ka intervals are associated with similar deviations ($-8 \pm 8.5^\circ$ and $-7.7 \pm 13.1^\circ$, respectively) indicates that the anomaly seems to be stable within the last 150 Kyr, although a large scatter of inclinations characterizes the 100–150 Ka subset. The mean value derived from the older data (>150 Ka) is characterized by an almost dipolar inclination ($\Delta I = -1.4 \pm 7.6^\circ$), but again, this determination has a large error. The mean field directions derived for these two subsets differ by 8.6°. The mean directions of each set have largely overlapping confidence circles, which, however, exclude the mean direction of the other set. This is the critical situation where it is difficult to decipher whether two data sets are, or are not, statistically distinct. The VGP scatter remains close to 14° in both cases, which would indicate that a significant amount of secular variation has been properly sampled and, therefore, that a representative mean direction has been obtained for each time period. Therefore, we conclude that there is a tendency toward steeper inclinations during most recent times. The difference in mean inclination would suggest that if persistent non-dipolar terms are involved, they would have a time constant on the order of 100–200 Kyr. This is compatible with the suggestion by Carlut *et al.* (2000) that variations of the mean field direction could be observed over a few hundreds of thousands years. Although it is based on a relatively small data set, Carlut *et al.* (2000) observed a significant difference in inclination anomaly between the 0–150 Ka and the 400–650 Ka time intervals at La Guadeloupe Island. Similarly, Zanella (1998) suggested, on the basis of a rather small data set too, that at Pantelleria (Sicily), the inclination anomaly of the past 50 Kyr was larger than earlier.

**Table 4.** Statistical tests on the Brunhes Indonesian data set.

| Data set | N | C1 | | C1-0 | | CJ98 | | CJ98-0 | |
|---|---|---|---|---|---|---|---|---|---|
| | | $\chi 2$ | KS | $\chi 2$ | KS | $\chi 2$ | KS | $\chi 2$ | KS |
| Indonesia, Brunhes | 36 | 0.25 | 0.48 | 0.25 | 0.50 | 0.9 | 0.52 | 0.47 | 0.29 |

Probabilities for the data to be incompatible with statistical models C1, CJ-98 and their counterpart with a zero mean quadrupolar term ($-0$), using $\chi 2$ and KS tests (approach implemented by Khokhlov *et al.* 2001).

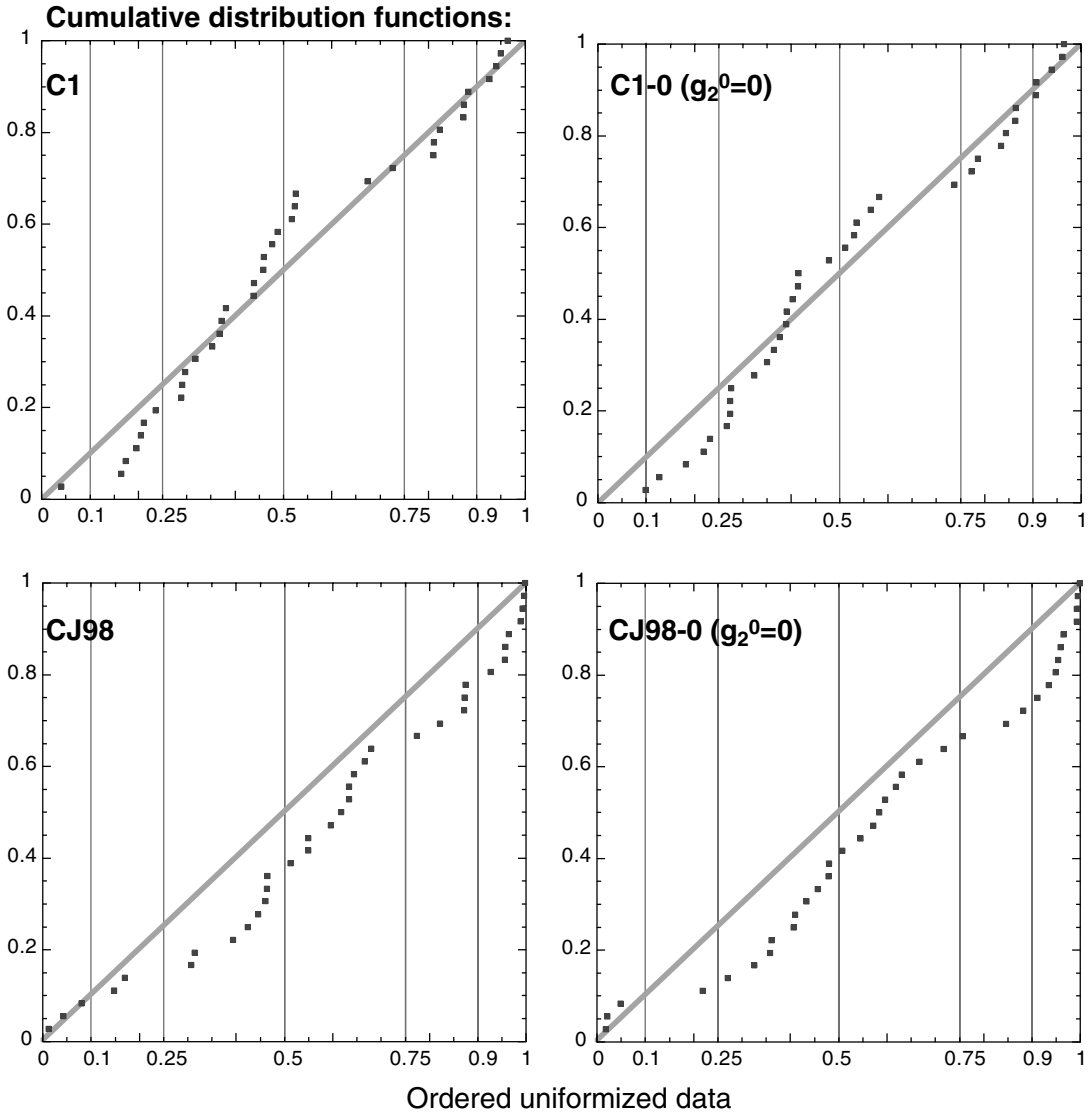


**Figure 9.** Empirical distributions of the uniformized Brunhes Indonesian data for the various models tested. The theoretical cumulative distribution function of a uniform distribution (1:1 line) is plotted as a grey line. The procedure of 1-D uniformization is described in Khokhlov *et al.* (2001). Corresponding probabilities for the $\chi 2$ and KS tests are given in Table 4.

## 8 CONCLUSIONS

36 independent drawings of the field during the Brunhes have been obtained from volcanic rocks in the Java and Bawean Islands. The mean field direction obtained for this data set is compatible with the direction predicted by a dipolar field model, as well as with the direction predicted by a persisting quadrupole of 5 per cent of the $g_1^0$. According to statistical models, a persistent quadrupolar term is not necessarily required to fit our data. The present results, with a mean Brunhes inclination anomaly of $-4.7^\circ \pm 5.3^\circ$, do not support the extension of the zone of negative inclination anomalies documented by the southwestern Pacific sediments studied by Elmaleh *et al.* (2001) toward the eastern Indian ocean. A larger anomaly of $-8 \pm 7.5^\circ$ would have prevailed during the past 150 Kyr, which raises the possibility that the time-averaged field may vary over hundreds of thousands of years. Dating of flows is in progress to provide further insights into the detailed temporal evolution of the Brunhes Earth magnetic field at the Java and Bawean Islands.

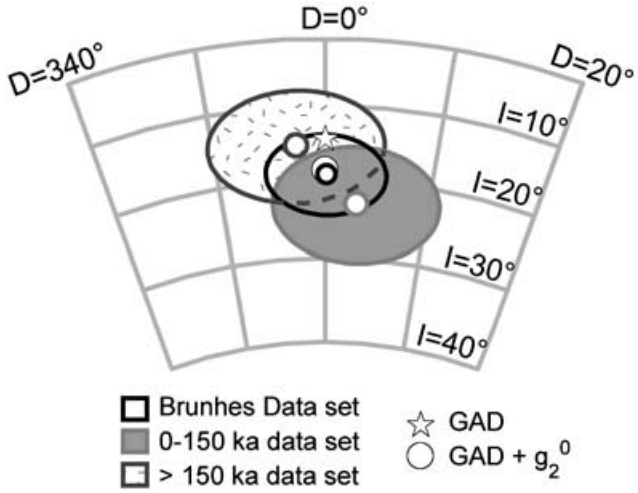


**Figure 10.** Equal area projection of the site mean directions with Fisherian 95 per cent confidence intervals, for a few temporal groups: the entire Brunhes chron, 150–0 Ka and >150 Ka (see Table 3). The directions predicted by a GAD model and a model including a persistent $g_2^0$ of 5 per cent of the GAD are plotted as a star and a large dot, respectively.

## ACKNOWLEDGMENTS

C. Widiwijayanti and M. Diament greatly assisted with the organization of the field trip in Indonesia and are warmly thanked. The authors also wish to thank R. Maury and M. Pubellier, as well as S. Andreastuti and the other members of the Merapi Volcano Observatory, as well as the members of the Volcanological Survey of Indonesia, who helped us prior to and during the field trip. The authors are grateful to G. Hulot who eased the use of the statistical tests and helped with data analysis, A. Roberts for a thorough review of an early version of the text, and N. Opdyke for his review. This work was supported by an INSU-CNRS Intérieur de la Terre programme. This is IPGP contribution N°1966.

## REFERENCES

Andreastuti, S.D., Alloway, B.V. & Smith, I.E.M., 2000. A detailed tephrostratigraphic framework at Merapi volcano, Central Java, Indonesia: implications for eruption prediction and hazard assessment, *J. Volc. Geotherm. Res.,* **100,** 51–67.

Audunsson, H. & Levi, S., 1989. Drilling-induced remanent magnetization in basalt drill cores, *Geophys. J. Int.,* **98,** 613–622.

Bahar, I., 1984. Contribution à la connaissance du volcanisme indonésien : le Merapi (Centre Java), cadre structural, pétrologie, géochimie et implications volcanologiques, *PhD thesis*, Université de Montpellier, Montpellier, France.

Bellon, H., Soeria-Atmadja, R., Maury, R.C., Euparka, E. & Yuwono, Y.S., 1990. Chronology and petrology of back-arc volcanism in Java, *Journal of Southeast Asian Earth Science,* **4,** 76–77.

Berthommier, P., 1990. Etude volcanologique du Merapi (Centre Java). Téphrotratigraphie et Chronologie. Mécanismes éruptifs, *PhD thesis*, Université Blaise Pascal, Clermont-Ferrand, France.

Camus, G., Gourgaud, A., Mossand-Berthommier, P.-C. & Vincent, P.-M., 2000. Merapi (Central Java, Indonesia): An outline of the structural and magmatological evolution, with a special emphasis to the major pyroclastic events, *J. Volc. Geotherm. Res.,* **100,** 139–163.

Carlut, J. & Courtillot, V., 1998. How complex is the time-averaged geomagnetic field over the past 5 Myr?, *Geophys. J. Int.,* **134,** 527–544.

Carlut, J., Quidelleur, X., Courtillot, V. & Boudon, G., 2000. Palaeomagnetic directions and K/Ar dating of 0–1 Ma flows from la Guadeloupe Island (French West Indies): Implications for time averaged field models, *J. geophys. Res.,* **105,** 835–849.

Chamot-Rooke, N. & Le Pichon, X., 1999. GPS determined eastward Sundaland motion with respect to Eurasia confirmed by earthquakes slip vectors at Sunda and Philippine trenches, *Earth planet. Sci. Lett.,* **173,** 439–455.

Cogné, J.-P., 2003. Paleomac: a Macintosh application for treating paleomagnetic data and making plate reconstructions, *Geochem. Geophy. Geosyst.,* **G**(1), 1007, doi: 10.1029/2001GC000227.

Constable, C.G. & Johnson, C.L., 1999. Anisotropic secular variation models : implications for geomagnetic field observables, *Phys. Earth planet. Int.,* **115,** 35–51.

Constable, C.G. & Parker, R.L., 1988. Statistics of the geomagnetic secular variation for the past 5 Myr, *J. geophys. Res.,* **93,** 11 569–11 581.

Elmaleh, A., Valet, J.P. & Herrero-Bervera, E., 2001. A map of the pacific geomagnetic anomaly during the Brunhes chron, *Earth planet. Sci. Lett.,* **193,** 315–332.

Fisher, R.A., 1953. Dispersion on a sphere, *Proc. R. Soc. Lond., A,* **217,** 295–305.

Genevey, A., Gallet, Y. & Boudon, G., 2002. Secular variation study from non-welded pyroclastic deposits from Montagne Pelée volcano, Martinique (West Indies), *Earth planet. Sci. Lett.,* **201,** 369–382.

Gubbins, D. & Kelly, P., 1993. Persistent patterns in the geomagnetic field over the past 2.5 Myr, *Nature,* **365,** 829–832.

Johnson, C.L. & Constable, C.G., 1996. Paleosecular variation recorded by lava flows over the last 5 Myr, *Phil. Trans. R. Soc. Lond., A.,* **354,** 89–141.

Johnson, C.L. & Constable, C.G., 1997. The time-averaged geomagnetic field: global and regional biases for 0–5 Ma, *Geophys. J. Int.,* **131,** 643–666.

Johnson, C.L. & Constable, C.G., 1998. Persistently anomalous Pacific geomagnetic fields, *Geophys. Res. Lett.,* **25,** 1011–1014.

Khokhlov, A., Hulot, G. & Carlut, J., 2001. Towards a self-consistent approach to palaeomagnetic field modelling, *Geophys. J. Int.,* **145,** 157–171.

Kirschvink, J., 1980. The least-squares line and plane and the analysis of paleomagnetic data: examples from Siberia and Morocco, *Geophys. J. R. astr. Soc.,* **62,** 699–718.

Mandea, M. & Macmillan, S., 2000. International Geomagnetic Reference Field—The Eighth Generation, *Earth, Planets, Space,* **52,** 1119–1124.

Mulyadi, E., 1992. Le complexe de Bromo-Tengger (Est Java, Indonésie): Etude structurale et volcanologique, *PhD thesis*, Université Blaise Pascal, Clermont-Ferrand, France.

Newhall, C.G. *et al.,* 2000. 10 000 Years of explosive eruptions of Merpai Volcano, Central Java : archaeological and modern implications, *J. Volc. Geotherm. Res.,* **100,** 9–50.

Quidelleur, X. & Courtillot, V., 1996. On low-degree spherical harmonic models of paleosecular variation, *Phys. Earth planet. Int.,* **95,** 55–78.

Quidelleur, X., Valet, J.P., Courtillot, V. & Hulot, G., 1994. Long-term geometry field for the last five million years: an updated secular variation database, *Geophys. Res. Lett.,* **21,** 1639–1642.

Schneider, D.A. & Kent, D.V., 1990. The time-averaged paleomagnetic field, *Rev. Geophys.,* **28,** 71–96.

Soeria-Atmadja, R., Maury, R., Bellon, H., Joron, J.-L., Yuwono, Y.S. & Cotten, J., 1988. Remarques sur la répartition du volcanisme potassique quaternaire de Java (Indonésie), *C. R. Acad. Sci. Paris, série II,* **307,** 635–641.

van Bemmelen, R.W., 1949. *The geology of Indonesia,* The Government Printing Office, The Hague, Netherlands.

Wirakusumah, A.D., Juwarna, H. & Loebis, H., 1989. *Peta Geologi Gunung Merapi Jawa Tengah (1 sheet, scale 1:50,000)*, Direktorat Vulkanologi, Bandung, Indonesia.

Zaennudin, A., 1990. The stratigraphy and nature of the stratocone of Mt Cemoro lawang in the Bromo Tengger caldera, East-Java, Indonesia, *MSc thesis*, Victoria University, Wellington, New Zealand.

Zaennudin, A., Handisantono, R.D., Erfan, R.D. & Mulyana, A.R., 1994. Peta Geologi Gunungapi Bromo-Tengger, Jawa Timur, Direktorat Vulcanologi, Bandung (1 sheet, Scale 1:50,000).

Zanella, E., 1998. Paleomagnetism of Pleistocene volcanic rocks from Pantelleria Island (Sicily Channel), Italy, *Phys. Earth planet. Int.,* **108,** 291–303.

Zijderveld, J.D.A., 1967. A.C. demagnetization of rocks: Analysis of results, in *Methods in Paleomagnetism*, pp. 254–286, eds Collinson, D.W., Creer, K.M. & Runcorn, S.K., Elsevier, New York.